Enhanced cycling stability of La modified $LiNi_{0.8-x}Co_{0.1}Mn_{0.1}La_xO_2$ for Li-ion battery

Ming-xia DONG, Xiang-qun LI, Zhi-xing WANG, Xin-hai LI, Hua-jun GUO, Zhen-jun HUANG

School of Metallurgy and Environment, Central South University, Changsha 410083, China

Abstract: A series of layered $LiNi_{0.8-x}Co_{0.1}Mn_{0.1}La_xO_2$ (x=0, 0.01, 0.03) cathode materials were synthesized by combining co-precipitation and high temperature solid state reaction to investigate the effect of La-doping on $LiNi_{0.8}Co_{0.1}Mn_{0.1}O_2$. A new phase $La_2Li_{0.5}Co_{0.5}O_4$ was observed by XRD, and the content of the new phase could be determined by Retiveld refinement and calculation. The cycle stability of the material is obviously increased from 74.3% to 95.2% after La-doping, while the initial capacity exhibits a decline trend from 202 mA·h/g to 192 mA·h/g. The enhanced cycle stability comes from both of the decrease of impurity and the protection of newly formed $La_2Li_{0.5}Co_{0.5}O_4$, which prevents the electrolytic corrosion to the active material. The CV measurement confirms that La-doped material exhibits better reversibility compared with the pristine material.

Key words: nickel-rich cathode material; La-doping; electrochemical property; cycle stability; Li-ion diffusion coefficient

1 Introduction

Lithium-ion batteries (LIBs) have been considered as one of the most promising candidates for the electric vehicles (EVs) and hybrid electric vehicles (HEVs). As one of the most promising cathode materials for LIBs, $LiNi_{0.8}Co_{0.1}Mn_{0.1}O_2$ has been studied intensively in the past decades because of its lower cost, higher capacity and environmentally-friendly characteristics compared with $LiCoO_2$. However, its structural stability, initial coulombic efficiency, rate capability and cycling performance are unsatisfactory to the growing demand for application [1−4]. These disadvantages may be associated with the similar radius of Ni^{2+} ion (0.69 Å) and Li^+ ion (0.76 Å), which can cause the cation mixing and deteriorate the electrochemical performance of the material. Another feasible reason is that the delithiated positive material undergoes a faster phase transformation into NiO-type rock salt phase, leading to the enlarged interfacial impedance and poor cyclic property. Various approaches, such as lattice doping, surface modification, tuning the material composition, and smart design of core-shell or concentration gradient structures, have been carried out to solve these problems. Among these approaches, incorporation of metal ions into the lattice

has been proved to be an effective way to significantly enhance the structural stability and electrochemical characteristics of Ni-rich cathode. The particle size distribution, crystal structure, electronic conductivity and rapid Li^+ diffusion can be optimized by the incorporation of the metal cations.

Rare earth elements have some outstanding features like high electric charge, large radius and high self-polarization ability; hence, attracting more and more attention in the past few years. ZHONG et al [5] reported that Ce-doped $LiNi_{1/3}Co_{1/3}Mn_{1/3}O_2$ achieved enhanced structural stability, better discharge capacity and good cyclic stability. MOHAN et al [6] proposed that La−Li co-substituted $LiLa_{x-y}Li_yNi_{1-x}O_2$ cathode exhibited improved capacity retention, rate capacity and decreased irreversible capacity. VALANARAS et al [7] reported that Eu-doped $LiCoO_2$ exhibited excellent reversible capacity and improved electrical conductivity. Among the rare earth elements, La as the second most abundant rare earth element in the world (32×10^{-6} in Earth's crust), possesses a relatively large radius and high affinity for oxygen. Consequently, La-doping process can enhance the conductivity and stability of the material. Several reports show that La^{3+} can effectively enhance electronic conductivity and improve structural stability of cathode material [8−10]. While few studies report the effect of

La-doping on $LiNi_{0.8}Co_{0.1}Mn_{0.1}O_2$ cathode material.

As we all known, the high temperature solid state reaction is the traditional way to achieve the doped material; however, this process often suffers from uneven doping, which results in the inhomogeneous performance of the material. In this work, $LiNi_{0.8-x}Co_{0.1}Mn_{0.1}La_xO_2$ (x=0, 0.01, 0.03) compounds were prepared through combination of co-precipitation method and high temperature solid state reaction, the La-doped materials were firstly synthesized during co-precipitation of precursor, and then completed the sintering process with $LiOH·H_2O$. The effects of La doping on the morphology and electrochemical properties of the $LiNi_{0.8}Co_{0.1}Mn_{0.1}O_2$ material were investigated.

2 Experimental

2.1 Synthesis of materials

Spherical Ni-rich $Ni_{0.8-x}Co_{0.1}Mn_{0.1}La_x(OH)_2$ (x=0, 0.01, 0.03) precursors were prepared by a continuous hydroxide co-precipitation method, employing a continuously stirred tank reactor (CSTR) under Ar atmosphere. 1 mol/L starting aqueous solution of $NiCl_2·6H_2O$, $CoCl_2·6H_2O$, $MnCl_2·4H_2O$ and $La(NO_3)_3·6H_2O$ was added into the reactor using a peristaltic pump. At the same time, amounts of NaOH solution (aq.) and NH_4OH solution (aq.) were also slowly pumped into the reactor as a chelation agent. The solution was maintained at 55 °C with continuous stirring for 4 h and the pH value of the solution was carefully controlled at 11.50±0.05. The precipitates were centrifuged and dried at 80 °C for 12 h. Finally, $LiOH·H_2O$ was mixed with the precursor (as the ratio of 1:1.05) by hand force grinding for 1 h. Then, the obtained mixture was sintered at 480 °C for 5 h, then sintered at 750 °C for 15 h under O_2 atmosphere. An excess of lithium was used to compensate for lithium loss during the calcination. Thus, La-substituted samples $LiNi_{0.79}Co_{0.1}Mn_{0.1}La_{0.01}O_2$ and $LiNi_{0.77}Co_{0.1}Mn_{0.1}La_{0.03}O_2$ were obtained and labeled as La1 and La3. For comparison, the pristine $LiNi_{0.8}Co_{0.1}Mn_{0.1}O_2$ sample (labeled as La0) was also prepared by the same processes.

2.2 Sample characterization

The crystallization and structure of the samples were characterized by X-ray diffraction (XRD, Rigaku, Rint−2000) with Cu K_α radiation. The morphology was obtained with field-scanning electron microscope (SEM, JEOL, JSM−5600LV) equipment. X-ray photoelectron spectroscopy (XPS, VG Multilab 2000) measurement was used to determine the surface chemical states of Ni, Co, Mn and La with Mg K_α radiation.

2.3 Electrochemical measurement

Electrochemical performance measurements were carried out with R2025 coin-type cells. The working electrodes were prepared as follows: a mixture of 80% active materials, 10% acetylene blacks, and 10% polyvinylidene fluoride (PVDF) binder were added in N-methyl pyrrolidinone to produce slurry. The obtained slurry was coated onto Al foil. Then, the foil was cut into disks and pressed under 15 MPa for 1 min then dry in a vacuum oven at 120 °C for 10 h. Circular electrodes (12 mm in diameter) were then punched out. The typical mass of the cathode ranged from 0.15 to 0.2 mg/cm^2 with the corresponding mass of active material range between 6 and 8 mg. The electrolyte was prepared by dissolving 1 mol/L $LiPF_6$ into ethylene carbonate (EC)-dimethyl carbonate (DMC)-ethyl methyl carbonate (EMC) (1:1:1 in volume). Galvanostatic charge−discharge tests were performed using NEWARE battery cycler. The measurement of cyclic voltammetry (CV) tests were carried out in a potential range of 2.8−4.3 V (vs Li$^+$/Li) at a scanning rate of 0.1 mV/s.

3 Result and discussion

The XRD patterns of La0, La1, La3 powders are shown in Fig. 1. For all samples, the characteristic peaks of a hexagonal α-NaFeO$_2$ structure with a space group of $R\bar{3}m$ of $LiNi_{0.8}Co_{0.1}Mn_{0.1}O_2$ can be identified. A clear splitting of the (0 0 6) / (0 1 2) and (0 1 8) / (1 1 0) peaks are presented even in the most heavily doped (x=0.03) sample, suggesting that the highly ordered layer structure is not disturbed by the introduction of La^{3+} into the $LiNi_{0.8}Co_{0.1}Mn_{0.1}O_2$ matrix. However, for La-doped samples, there are several weak peaks between 24° and 36°, which can be indexed to La-containing perovskite phases $La_2Li_{0.5}Co_{0.5}O_4$ by comparing with JCPDF card (JCPDS File No. 01−083−1844), and the intensity of the peak increases with the increase of La content.
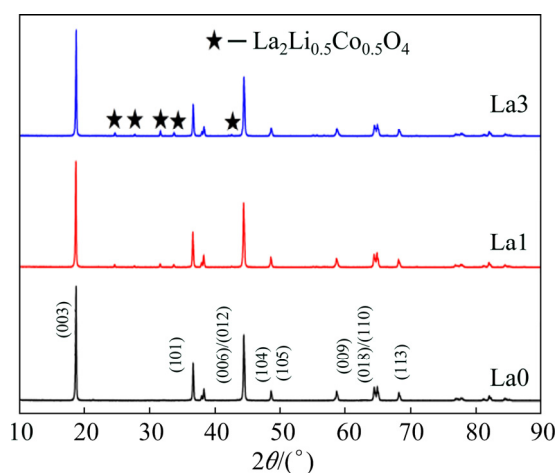

Fig. 1 XRD patterns of as-prepared samples La0, La1, La3

In order to further confirm the effect of La^{3+} on the crystal structure of the material, Rietveld refinements were carried out and the results are shown in Fig. 2. Firstly, the theoretical and calculated molecular fractions of all sample are shown in Table 1. It can be seen from Table 1 that the molecular fractions of $LiNi_{0.8}Co_{0.1}Mn_{0.1}O_2$ phase and $La_2Li_{0.5}Co_{0.5}O_4$ phase are different after La-doping process. For the La1 sample, the theoretical fraction of $La_2Li_{0.5}Co_{0.5}O_4$ is 1%, while the calculated datum from experimental is 0.60%. Identically, the La3 sample shows the similar result, which suggests that the La element is successfully incorporated into crystalline host lattice. In addition, the results of Rietveld refinement of La0, La1, La3 powers are shown in Table 2. Values of the parameters wR_p and R_p for all samples are within 15, ensuring the reliability of the refinement results. It can be observed that the cell parameter c decreases while the parameter a shows little change with the addition of La, which suggests a more stable layered structure. While the cation mixing shows an increase trend, suggesting that the layer structure is certainly damaged by La doping, which is due to the fact that the formation of new phase consumes part of the Li, resulting in a larger amount of the Li vacancy in the lattice.

XPS was carried out to explore the valence states of Ni, Co, Mn and La ions on the surface of the prepared samples. Figure 3(a) exhibits the XPS spectra for La. The measured binding energy for La 3d is around 835.49 eV, indicating that the La ion exists at the valance state of +3. With the increase of La substitution for Ni, the intensity of the La 3d gradually increased, implying that the concentration of La^{3+} increased [11,12]. Figure 3(b) shows the XPS spectra of Ni ions. The main peaks of Ni $2p_{3/2}$ peak shift from lower binding energy of 854.69 eV to higher binding energy of 855.39 eV with the increasing amount of La^{3+}, indicating an enhanced amount of Ni^{4+} ions present on the surface. Simultaneously, the enhanced capacity for La1 sample was explained. The valence states of the element Co change between +2 and +3, as shown in Fig. 3(c), the main peak of Co $2p_{3/2}$ and Co $2p_{1/2}$ are at 780.09 eV and 794.99 eV, respectively. The binding energy difference between Co $2p_{1/2}$ and Co $2p_{3/2}$ is about 14.10 eV, which indicates that the Co ions are mainly in an oxidation state of +3. In addition, the ratio of Co^{3+} ions is 6.88% for La0, 7.10% for La1 and 9.49% for La3, respectively. The Mn XPS spectra are shown in Fig. 3(d), two broad main peaks are observed at about 654.69 eV and 642.59 eV, which is attributed to Mn $2p_{3/2}$ and Mn $2p_{1/2}$ [13], indicating the Mn element in the crystal lattice is mainly +4 valance.
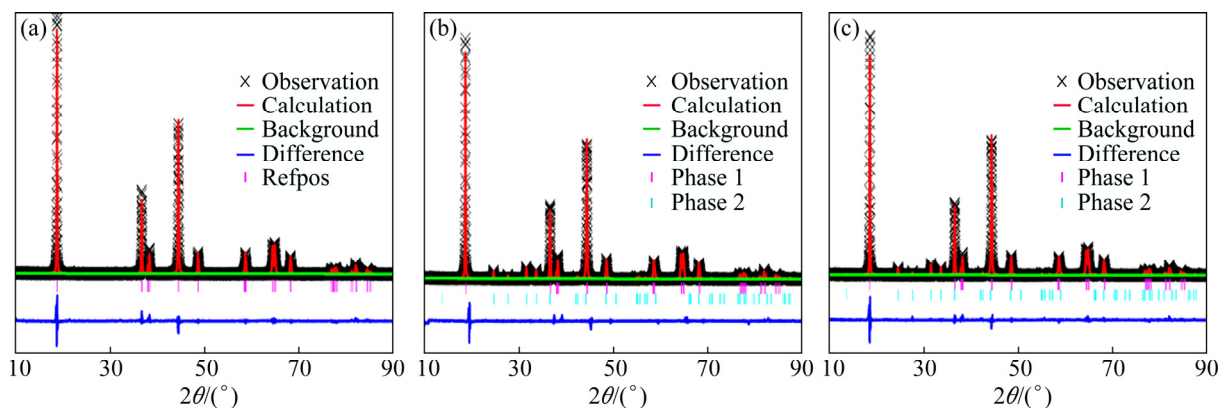

Fig. 2 Rietveld refinement results for prepared samples: (a) La0; (b) La1; (c) La3

Table 1 Theoretical and calculated molecular fractions of all samples

Phase	Theoretical fraction/%			Calculated fraction/%		
	x=0	x=0.01	x=0.03	x=0	x=0.01	x=0.03
$LiNi_{0.8}Co_{0.1}Mn_{0.1}O_2$	100	99.00	97.00	100	99.40	99.38
$La_2Li_{0.5}Co_{0.5}O_4$	0	1.00	3.00	0	0.60	0.62

Table 2 Results of Rietveld refinement of L0, La1, La3 powders

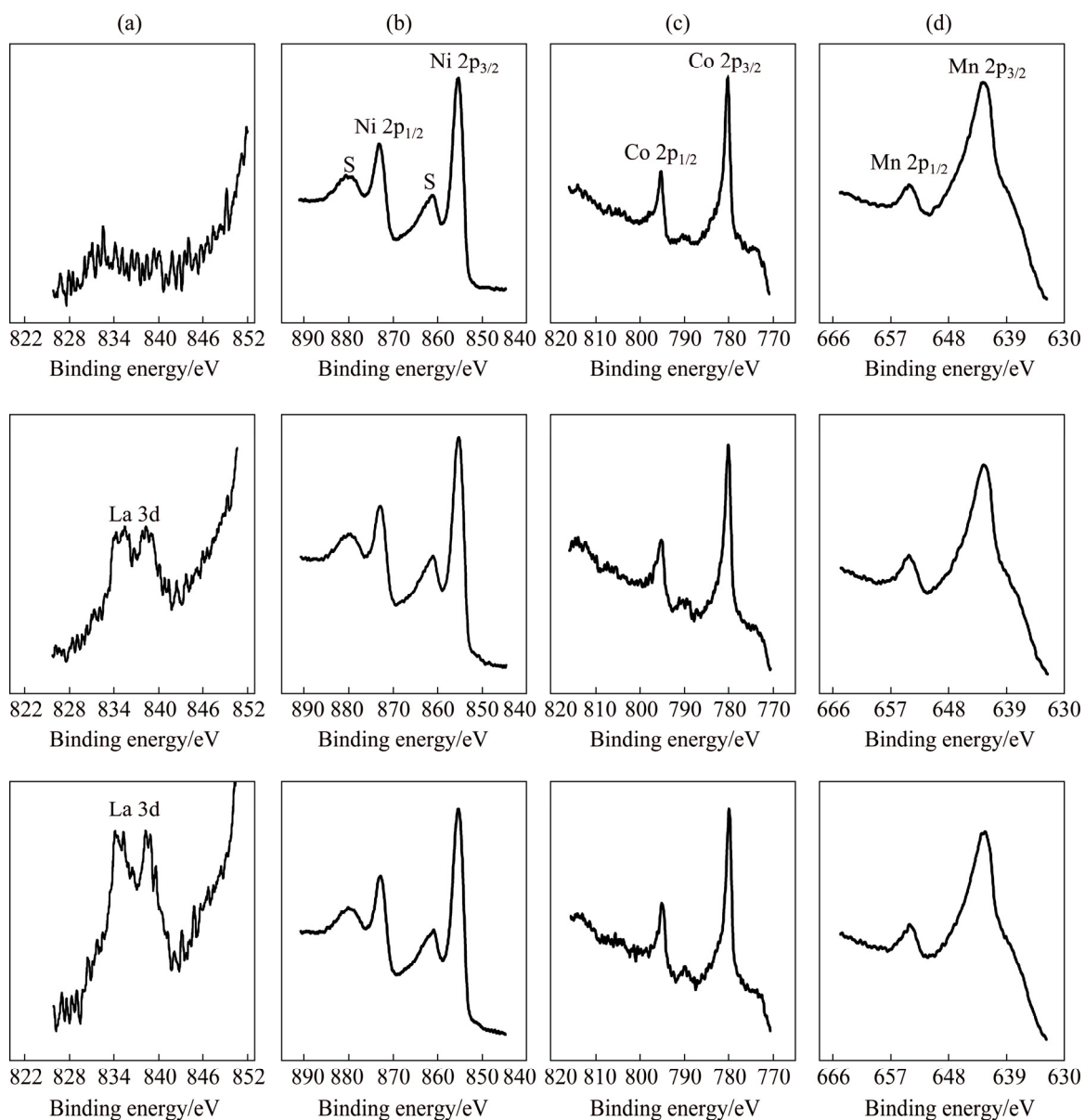| x	Occupation				a/Å	c/Å	V/Å³	wR_p	R_p
	Li1	Ni1	Li2	Ni2					
0	0.9842	0.0158	0.0158	0.7842	2.8710	14.2087	101.426	13.72	10.35
0.01	0.9803	0.0197	0.0197	0.7803	2.8709	14.2005	101.358	11.78	8.82
0.03	0.9836	0.0164	0.0164	0.7836	2.8712	14.2013	101.388	12.56	9.18

Fig. 3 XPS spectra of La 3d (a), Ni 2p (b), Co 2p (c), Mn 2p (d) for prepared samples

Typical powder morphology and components of the sample La0, La1, La3 were investigated by SEM which are shown in Figs. 4(a₁−a₂), (b₁−b₂) and (c₁−c₂). It can be found that all samples exhibit a spherical-like sharp, and the La-doped samples show much smaller particle size, which could make the nucleation process faster or easier, consequently forming a large number of nuclei in a shorter time, leading to a smaller and more uniform particle size. So, La^{3+} doping is beneficial to inhibiting the crystal growth. And the decreased particle size will shorten the lithium diffusion distance, which is helpful to the reversible intercalation/de-intercalation process. This is also in agreement with the previous report by DONG et al [14].

The corresponding EDS analyses of all samples are shown in Figs. 4(a₃)−(c₄). Among all the La-doped samples, La element can be observed. The peak intensity increases with the increase of La content, confirming the actual presence of La in $LiNi_{0.8}Co_{0.1}Mn_{0.1}O_2$.

To estimate the influence of La-doping on the electrochemical performances of the material, the initial charge−discharge curves of all samples were carried out at $0.1C$ ($1C$=200 mA/g) between 2.8 and 4.3 V (vs Li$^+$/Li) at room temperature, the results are shown in Fig. 5(a). It can be found that the charge capacities of the samples increase firstly and then decrease with the substitution of Ni by La. The La0 sample exhibits the highest initial discharge capacity of 203 mA·h/g, and the corresponding values for La1 and La3 samples are 206 and 192 mA·h/g. At the same time, the La1 sample exhibits the highest coulombic efficiency of 206 mA·h/g at $1C$. At the same time, the La1 sample exhibits the highest coulombic efficiency of 89.35%. The corresponding capacities for La0 and La3 samples are 88.86% and 85.56%.
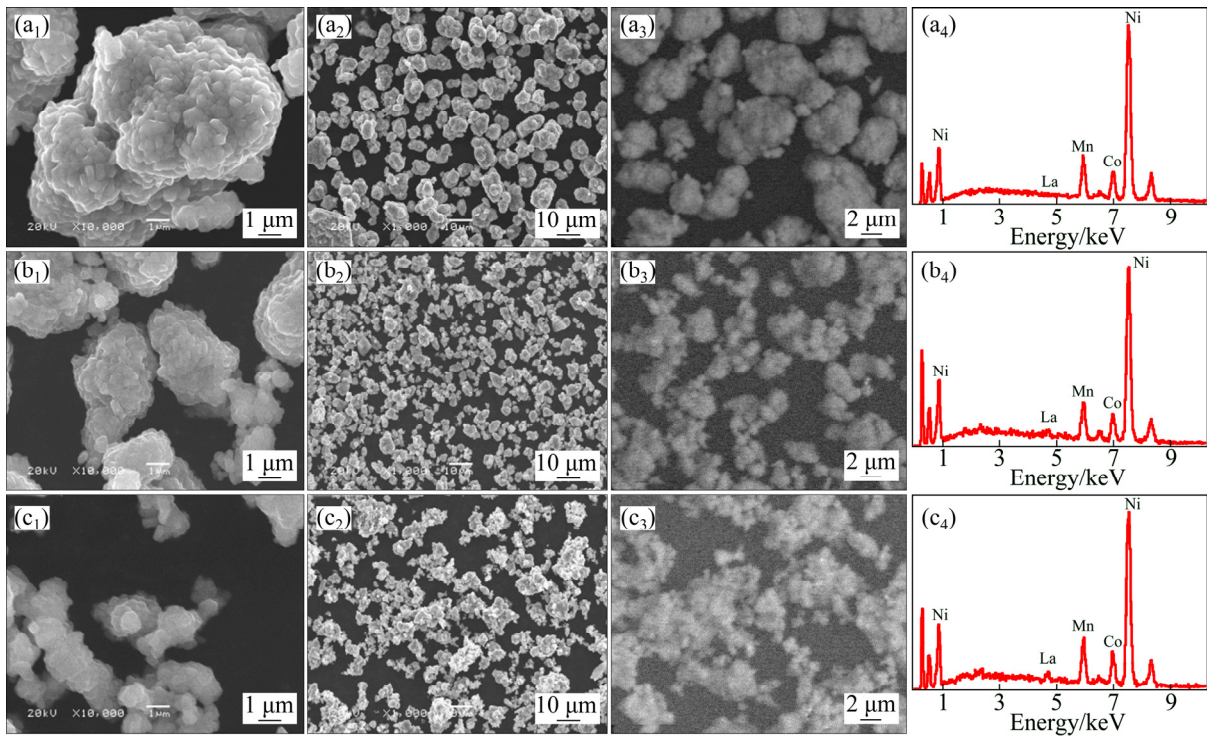
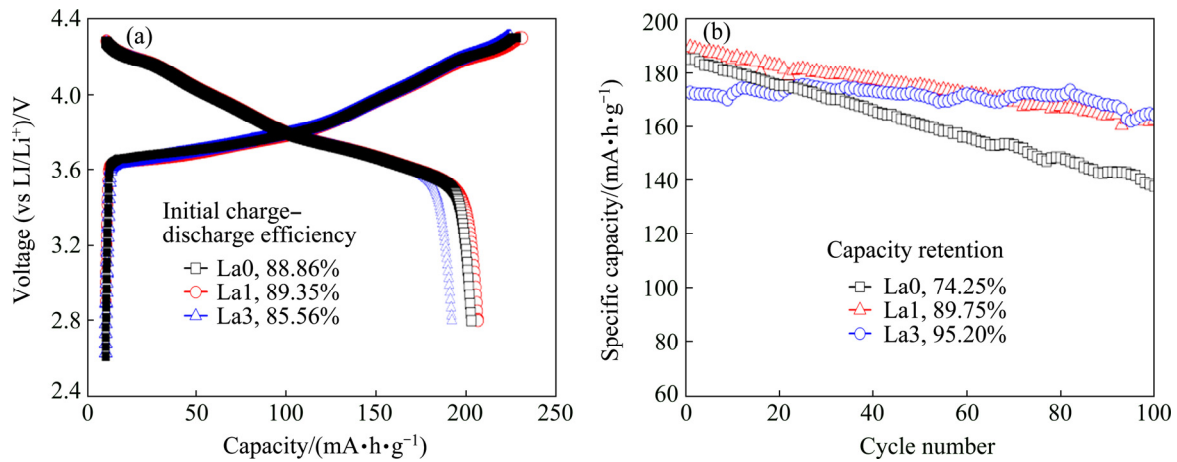**Fig. 4** SEM and EDS images of prepared samples La0 (a), La1 (b), La3 (c)

Fig. 5 Initial charge−discharge curves of La0, La1, La3 (a), cycle performance of La0, La1 and La3 at 1C (b)

Consequently, the La-doped samples exhibit a lower initial coulombic efficiency than that of the La0 sample, which suggests that the irreversible capacity is increased by La-doping during the first cycle.

The cycle performances of all samples are shown in Fig. 5(b), which is carried out at the current density of 200 mA·h/g. It can be found that the capacity retentions of La1 and La3 significantly increase comparing with that of La0 after 100 cycles. The capacity retentions of La0, La1, La3 samples are 74.25%, 89.75% and 95.20%, respectively. One of the possible reasons is the formation of the perovskite phases ($La_2Li_{0.5}Co_{0.5}O_4$) with increasing La content in the compounds, which exists as the function of cover and protects the active material

from the corrosion of electrolyte.

The rate capabilities of all samples at different rates between 2.8 and 4.3 V are shown in Fig. 6. The cells were all charged/discharged at the rate from 0.1C to 5C, every process continued for 5 cycles. The result revealed that when discharged at low rate, no significant change in the capacity of the cells is exhibited. The plateaux of the profile become lower with the increase of current density. When the current density comes to 5C, the capacities for all the samples showed a dramatic drop. The test result shows that the La3 sample exhibits the best discharge capacity at high rate.

The Li$^+$ diffusion coefficient is important to rate capability of the cathode materials, thus the Li$^+$ diffusion
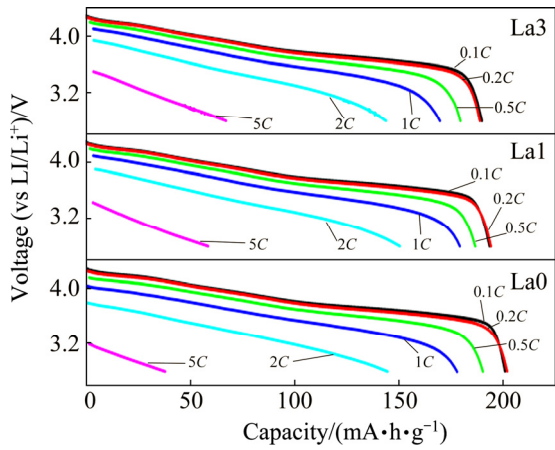
Fig. 6 Rate capability of prepared samples La0, La1, La3

coefficients of all samples are confirmed by GITT technology [15−17]. GITT is an effective way to investigate the chemical diffusion coefficient, which is

based on chronopotentiometry under an approximate thermodynamic equilibrium conditions. The D_{Li}^+ can be calculated with Eq. (1) [15].

$$D_{Li^+} = \frac{4}{\pi}\left(\frac{m_B V_m}{M_B S}\right)^2 \left(\frac{\Delta E_s}{\tau(dE_\tau/d\sqrt{\tau})}\right)^2 \quad (\tau \ll L^2/D_{Li^+}) \quad (1)$$

where m_B represents the mass of the active material (g), V_m stands for the molar volume of the samples, M_B is the relative molecular mass of the sample, S is the area of the electrode, τ stands for the time duration in the process of the current pulse, ΔE_s exhibits the difference in the steady state voltage at a single-step GITT experiment, and L represents the length of Li^+ ions diffusion.

Figures 7(a)−(c) show the GITT curves of the fourth discharge cycle, all the samples are discharged at a Galvano static current of 0.1C for 10 min, and then rest for 50 min to reach a quasi-steady-state, this process repeated from 4.3 V to 2.8 V. Figures 7(d)−(f) show a typical GITT profile for each sample during a single
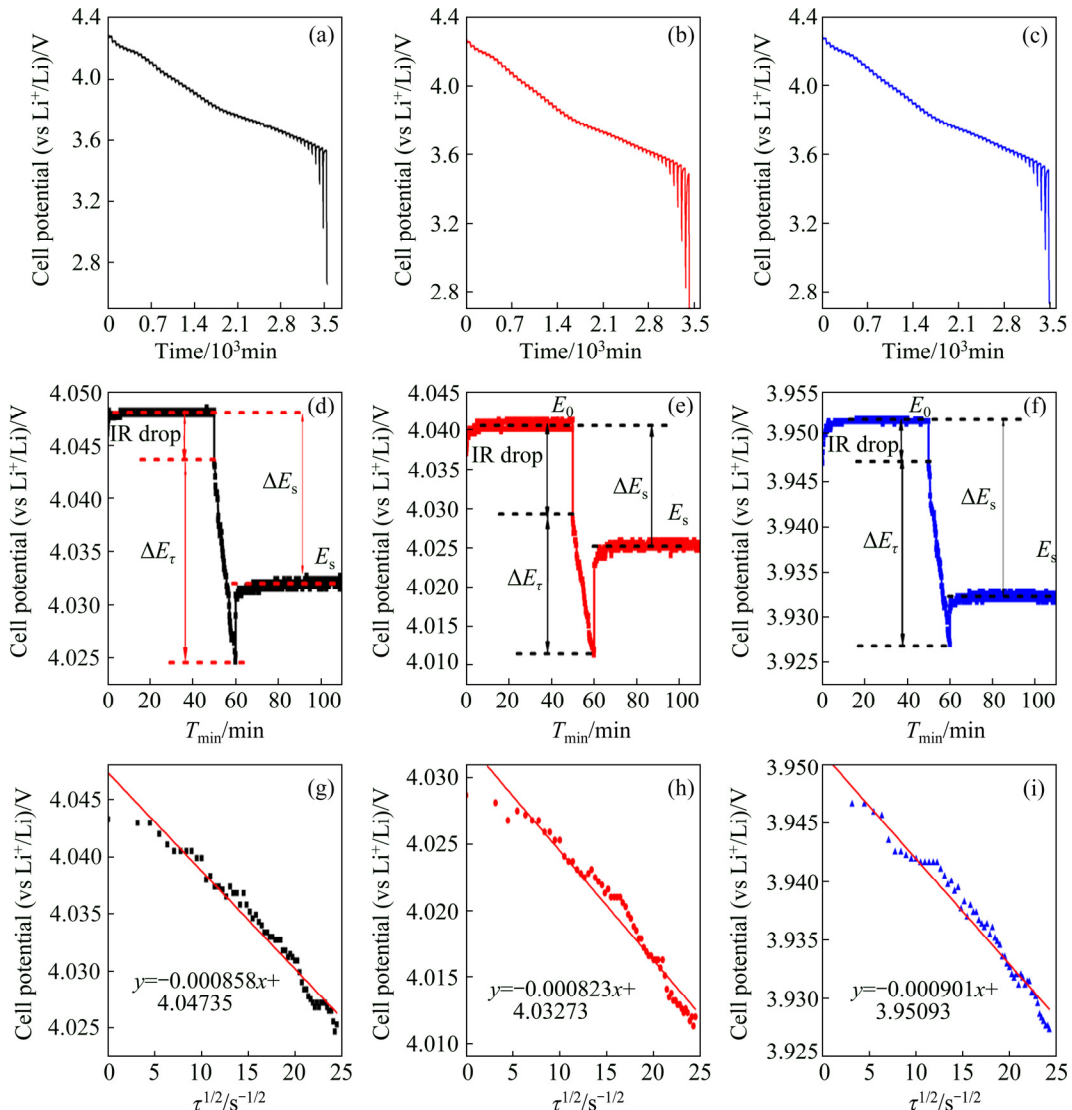

Fig. 7 GITT curves of La0, La1, La3 as function of time in voltage range of 2.8−4.3 V (a−c), scheme for single titration step of GITT curves (d−f), linear fit of the cell voltage as function of square root of time ($\tau^{1/2}$) with different pulse currents (g−i)

GITT experiment step where schematically reveal different parameters E_0, E_s, E_τ, ΔE_s, τ, etc. Figures 7(g)−(i) represent the responding potential (E) of each tested cell as a function of $\tau^{1/2}$ for the single GITT curve. It can be observed that the relationship between E and $\tau^{1/2}$ shows a straight line trend, thus the Eq. (1) can be simplified as

$$D_{Li^+} = \frac{4}{\pi\tau}\left(\frac{m_B V_m}{M_B S}\right)^2\left(\frac{\Delta E_s}{\Delta E_\tau}\right)^2 \quad (\tau \le L^2/D_{Li^+}) \qquad (2)$$

From the obtained GITT data, and combined with the Eq. (2), the $\lg(D_{Li^+})$ for all samples, as a function of potential, is shown in Fig. 8. It can be found that all samples show similar curves, suggesting that La doping does not influence the mechanism of the Li ions extraction from structure. Combined with the calculation result, the minimum values of D_{Li^+} exhibit at the plateau region. For the La0 sample, the stable D_{Li^+} values lie in about 1.4×10^{-9} cm²/s under 3.63 V and then decreases to 1.4×10^{-11} cm²/s with the cell potential drop to 3.56 V. The La1 samples exhibit the highest D_{Li^+} values of 3.62×10^{-9} cm²/s around 3.59 V. and decrease to 1.71×10^{-10} cm²/s with the cell potential dropped to 3.55 V, and the La3 sample shows similar result with La1 sample. The result shows that with the addition of La, the D_{Li^+} values increase obviously. Because of the Li⁺ diffusion coefficient is in associate with the rate capacity. Therefore, the La-doped samples exhibit better rate performance due to the increase of the rate of Li⁺ diffusion.
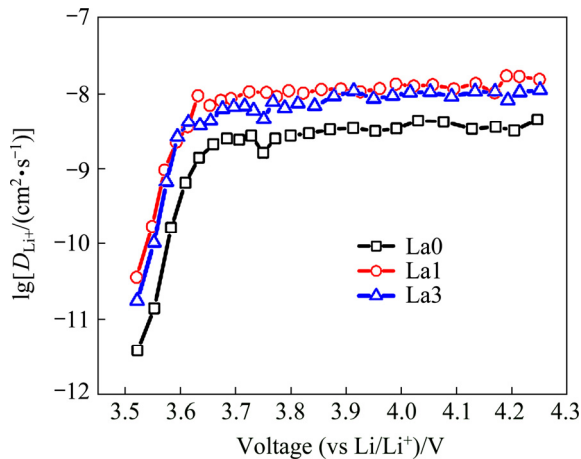
Fig. 8 Chemical diffusion coefficients of Li⁺ as function of potential for as-prepared samples

Cyclic voltammetry (CV) measurements were carried out to compare electrochemical behavior of the La0, La1, La3 electrodes. The peak potentials and peak current in the CV curve represent the electrochemical characteristics of the materials and reveal the phase transitions that occur during detercalation/intercalation of Li ions [18]. As shown in Fig. 9, no cathodic peaks near 3V region for all samples are observed, which indicates
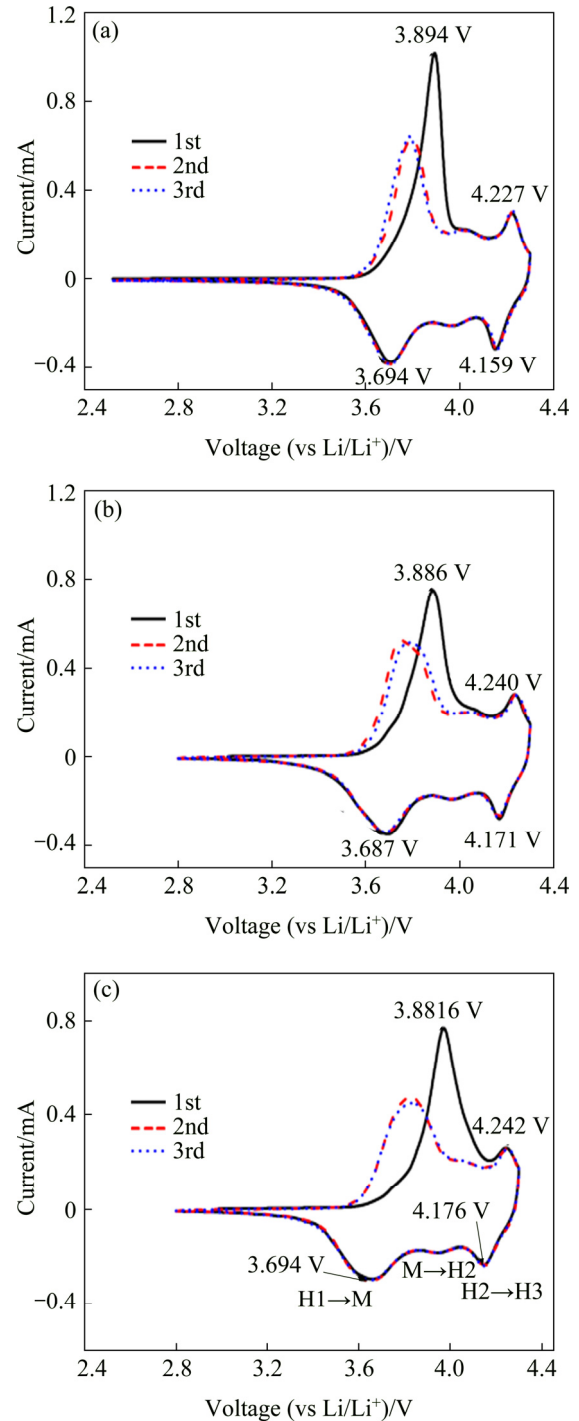
Fig. 9 CV curves for the first 3 cycles of prepared samples: (a) La0; (b) La1; (c) La3

that there is no reduction of Mn^{3+}/Mn^{4+}, agreeing with previous studies [19,20]. It is also found that the difference of the curves between the first and second cycle decreased significantly by La substitution. In addition, the CV profile of the first cycle differs from those of the following cycles for all samples. The CV curves in the first cycle show three pairs of redox peaks, corresponding to the multiphase transition of hexagonal to monoclinic (H1→M), monoclinic to hexagonal

(M→H2), and hexagonal to hexagonal (H2→H3). As to the La0 sample, the anodic peak can be observed at ~3.894 V, and the corresponding cathodic peaks located at ~3.694 V. The difference of the main peak is 0.200 V. For the La-doped samples, the difference of the main peak is 0.199 V (La1) and 0.192 V (La3), which indicates a decreased polarization for La1 and La3 samples. Moreover, for La-doped materials, the curves of the second and third cycle almost overlap, which confirms the good reversibility during the cycling process, and it can be helpful to the cycle performance of the material.

4 Conclusions

1) Nickel-rich layered materials $LiNi_{0.8−x}Co_{0.1}Mn_{0.1}La_xO_2$ (x=0, 0.01, 0.03) have been prepared via combining co-precipitation method and high-temperature solid method.

2) The capacity retentions are significantly improved from 74.3% of La0 to 95.2% for La3, the rate capacity is also optimized after doping.

3) XRD analysis and Rietveld refinement results confirm the existence of La in the host structure, generating of the second phase leads to the improvement of cycle performance.

4) The results of GITT technology combined with the calculation confirm that the addition of La into the original material can significantly improve the Li^+ diffusion coefficients, verifying the improvement of rate capacity.

5) The result of cyclic voltammetry certifies the enhancement of the reversibility of the modified material.

References

[1]   SUN Y K, MYUNG S T, BANG H J, PARK B C, PARK S J, SUNG N Y. Physical and electrochemical properties of Li[Ni$_{0.4}$Co$_x$Mn$_{0.6−x}$]O$_2$ (x=0.1−0.4) electrode materials synthesized via coprecipitation [J]. Journal of The Electrochemical Society A, 2007, 154(10): 937−942.

[2]   WANG Jie-xi, LIU Zhao-meng, YAN Guo-chun, LI Hang-kong, PENG Wen-jie, LI Xin-hai, SONG Liu-bin, SHIH K. Improving the electrochemical performance of lithium vanadium fluorophosphate cathode material: Focus on interfacial stability [J]. Journal of Power Sources, 2016, 329: 553−557.

[3]   YAN Guo-chun, LI Xin-hai, WANG Zhi-xing, GUO Hua-jun, WANG chao. Tris (trimethylsilyl) phosphate: A film-forming additive for high voltage cathode material in lithium-ion batteries [J]. Journal of Power Sources, 2014, 248(4): 1306−1311.

[4]   WANG Jie-xi, LI Xin-hai, WANG Zhi-xing, HUANG Bin, WANG Zhi-guo, GUO Hua-jun. Nanosized LiVPO$_4$ F/graphene composite: A promising anode material for lithium ion batteries [J]. Journal of Power Sources, 2014, 251(2): 325−330.

[5]   ZHONG Sheng-kui, WANG You, LIU Jie-qun, WAN Kang, LU Fan. Synthesis and electrochemical properties of Ce-doped LiNi$_{1/3}$Mn$_{1/3}$Co$_{1/3}$O$_2$ cathode material for Li-ion batteries [J]. Journal of Rare Earths, 2011, 29 (9): 891−895.

[6]   MOHAN P, KALAIGNAN G. PARUTHIMAL. Electrochemical performances of co-substituted (La and Li) LiLa$_{x−y}$Li$_y$Ni$_{1−x}$O$_2$ cathode materials for rechargeable lithium-ion batteries [J]. Materials Research Bulletin, 2013, 48 (9): 3049−3057.

[7]   VALANARASU S, CHANDRAMOHAN R, SOMASUNDARAM R M, SRIKUMAR S R. Structural and electrochemical properties of Eu-doped LiCoO$_2$ [J]. Journal of Materials Science-Materials in Electronics, 2011, 22(2): 151−157.

[8]   LIU Li-ying, LEI Xing-ling, TANG Hui, ZENG Ren-ren, CHEN Yi-ming, ZHANG Hai-ya. Influences of La doping on magnetic and electrochemical properties of Li$_3$V$_2$(PO$_4$)$_3$/C cathode materials for lithium-ion batteries [J]. Electrochimica Acta, 2015, 151: 378−385.

[9]   CHO Y D, FEY G T K, KAO H M. Physical and electrochemical properties of La-doped LiFePO$_4$/C composites as cathode materials for lithium-ion batteries [J]. Journal of Solid State Electrochemistry, 2008, 12(7−8): 815−823.

[10]   BAI Yu-jun, GONG Chen, QI Yong-xin, LUN Ning, FENG Ju. Excellent long-term cycling stability of La-doped Li$_4$Ti$_5$O$_{12}$ anode material at high current rates [J]. Journal of Materials Chemistry, 2012, 22(36): 19054.

[11]   DAVO B, de DAMBORENEA J J. Use of rare earth salts as electrochemical corrosion inhibitors for an Al−Li−Cu (8090) alloy in 3.56% NaCl [J]. Electrochimica Acta, 2004, 49(27): 4957−4965.

[12]   SCHLAPBACH L. XPS/UPS study of the oxidation of La and LaNi$_5$ and of the electronic structure of LaNi$_5$ [J]. Solid State Communications, 1981, 38(2): 117−123.

[13]   NESBITT H W, BANERJEE D. Interpretation of XPS Mn (2p) spectra of Mn oxyhydroxides and constraints on the mechanism of MnO$_2$ precipitation [J]. American Mineralogist, 1998, 83(3−4): 305−315.

[14]   DONG Yue, ZHANG Wen-long, WANG Chun-mei, SHI Ting, CHEN Li. Synthesis of La-doped Li$_2$MnSiO$_4$ nano-particle with high-capacity via polyol-assisted hydrothermal method [J]. Electrochimica Acta, 2015, 166: 40−46.

[15]   WEPPNER W, HUGGINS R A. Determination of the kinetic parameters of mixed‐conducting electrodes and application to the system Li$_3$Sb [J]. Journal of The Electrochemical Society, 1977, 124(10): 1569−1578.

[16]   WANG Jie-xi, LI Xin-hai, WANG Zhi-xing, GUO Hua-jun, HUANG Bin, WANG Zhi-guo, YAN Guo-chun. Systematic investigation on determining chemical diffusion coefficients of lithium ion in Li$_{1+x}$VPO$_4$F (0≤x≤2) [J]. Journal of Solid State Electrochemistry, 2015, 19(1): 153−160.

[17]   DEISS E. Spurious chemical diffusion coefficients of Li$^+$ in electrode materials evaluated with GITT [J]. Electrochimica Acta, 2005, 50(14): 2927−2932.

[18]   MAUGER A, JULIEN C. Surface modifications of electrode materials for lithium-ion batteries: Status and trends [J]. Ionics, 2014, 20(6): 751−787.

[19]   LI Ling-jun, LI Xin-hai, WANG Zhi-xing, GUO Hua-jun, YUE Peng, CHEN Wei, WU Ling. Synthesis, structural and electrochemical properties of LiNi$_{0.79}$Co$_{0.1}$Mn$_{0.1}$Cr$_{0.01}$O$_2$ via fast co-precipitation [J]. Journal of Alloys and Compounds, 2010, 507(1): 172−177.

[20]   PAULSEN J M, LARCHER D, DAHN J R. O$_2$ Structure Li$_{2/3}$[Ni$_{1/3}$Mn$_{2/3}$]O$_2$: A new layered cathode material for rechargeable lithium batteries [J]. Journal of the Electrochemical Society, 2000, 147 (8): 2862−2867.

循环性能改善的 La 改性锂离子电池材料 LiNi$_{0.8-x}$Co$_{0.1}$Mn$_{0.1}$La$_x$O$_2$

董明霞，李向群，王志兴，李新海，郭华军，黄振军

中南大学 冶金与环境学院，长沙 410083

摘　要：结合共沉淀法和高温固相法合成了一系列 La 掺杂的层状氧化物正极材料 LiNi$_{0.8-x}$Co$_{0.1}$Mn$_{0.1}$La$_x$O$_2$(x=0，0.01，0.03)，研究 La 对 LiNi$_{0.8}$Co$_{0.1}$Mn$_{0.1}$O$_2$ 材料的影响。通过 XRD 数据观察到了 La$_2$Li$_{0.5}$Co$_{0.5}$O$_4$ 新相的生成，通过 Rietveld 精修软件计算了第二相的含量。电化学性能测试结果表明 La 掺杂之后材料的循环稳定性从 74.3%上升到 95.2%，而首次比容量从 202 mA·h/g 降低到了 192 mA·h/g，循环稳定性的提高可以归因于新相的产生一方面消耗了材料中的杂质，另一方面粘附在颗粒表面保护材料不受电解液的腐蚀。CV 测试结果表明与未掺杂的材料相比，掺杂后的样品电化学可逆性更好。

关键词：高镍正极材料；La 掺杂；电化学性能；循环稳定性；锂离子扩散系数

(Edited by Xiang-qun LI)